Porosity effect on ZrO_2 hollow shell and hydrothermal stability for catalytic steam reforming of methane

Zi-Yian Lim,[a,b] Chunzheng Wu,[a] Wei Guo Wang,[a] Kwang-Leong Choy,[c] and Hongfeng Yin[a]

a Ningbo Institute of Material Technology and Engineering, 519 Zhuangshi Road, Zhenhai District, Ningbo 315201, China. E-mail: yinhf@nimte.ac.cn

b University of Nottingham, Ningbo China, 199 Taikang East Road, University Park, Ningbo 315100, China. E-mail: zx08427@nottingham.edu.cn

c UCL Institute for Materials Discovery, University College London, Kathleen Lonsdale Building, Gower Place, London, WC1E6BT, United Kingdom. E-mail: k.choy@ucl.ac.uk. Tel: +44(0) 207679 3855

Abstract

Hydrogen is an emerging energy source/carrier for oil refining and fuel cell applications. The development of an efficient and stable catalyst to produce hydrogen-rich gas is required for industrial application. Ni@yolk-ZrO_2 catalyst could be a potential solution to tackle the challenges in hydrogen production. The catalyst was characterized using a combination of XRD, TEM, AAS, TPR, BET, and XPS. In this study, the amount of micropores in ZrO_2 hollow shell was demonstrated to influence the catalytic performance. The catalysts were evaluated on time stream and identified its porosity effect on ZrO_2 hollow shell. From the characterization of BET and catalytic evaluation, the physical information of the ZrO_2 hollow shell was established, which affected the catalytic performance in steam reforming of methane. Furthermore, the results from XPS and TEM showed Ni particles were controlled under the ZrO_2 yolk-shell structure framework and showed the characteristic of moderately strong hydrothermal stability after steam reforming test. The catalysts were studied under GHSV of 50,400 $mLg_{cat}^{-1}h^{-1}$ and S/C=2.5 at 750°C and they maintained stable with methane conversion more than 90% for 48 hours.

1. Introduction

In spite of the necessity to move towards renewable chemical resources in the future, the importance of large fossil fuel, especially natural gas based will remain vital for number of years. Therefore, the development of robust and efficient catalyst is a priority today. Steam reforming of methane (SRM) has attracted industrial interest because of the possibility to convert widely available carbon-based substances into feedstock for further chemical processes.[1, 2] Despite the drawbacks of the steam reforming of methane tied to its high endothermic reaction, this process produces hydrogen-rich synthetic gas. Since the SRM reaction runs at high temperatures, highly thermo-stable catalysts have to be developed to feed industry requirement. Ni-based catalysts have been considered to be a promising candidate due to their low cost and availability.[3] However, these catalysts suffered fast deactivation at high temperature due to sintering or particle growth and formation of inactive carbon fibres/filaments. These drawbacks become main barrier in industrial applications.

Regarding the influence of the support on activity of the Ni-based catalysts, many studies have been reported. Doping with alkaline earth[4, 5] and rare earth[6-8] elements or substitute as substrate[9-11] have been considered to be promising strategies to promote nickel particle stability taking advantage of strong metal-support interactions. Other supports, in particular mesoporous structures[12-14] were demonstrated to effectively disperse and confine active metal particles in the mesoporous channels. Still, nickel particles' growth at high temperature during pre-treatment and catalytic process severely hurt for the process of steam reforming of methane.[15, 16] Therefore, the support should effectively promote uniform distribution of the Ni particles and show thermal stability to support Ni particles.

The coking mechanism is well studied, as carbon severely deposited in the catalyst will eventually lead to deactivation because the sintering of the active metal particles was

dependent on the selection of the supports. A study showed highly dispersed Ni nano-clusters in MCM-41 have high stability in carbon dioxide reforming of methane under high temperature.[17] The improved catalytic performance was suggested to be the result of high active centres on the pore wall surface and the stabilized dispersion of these active sites by the silica matrix. However, carbon deposition in mesoporous channel support is inevitable. Many studies show doping of other metals could suppress the growth of active metal in the mesoporous channel and lead to less carbon formation.[18-20]

Other approaches include the design of the support texture as core-shell or yolk-shell catalysts have also been reported recently.[21-26] These structures incorporate unique properties to prevent agglomeration of active metal nanoparticles. The structures were designed to encapsulate active metal with highly permeable shell to obtain reactant gaseous exchange and isolation of active metal simultaneously.[27] Many have demonstrated the effect of core-shell or yolk-shell structured supports[28-31] in catalyst applications. They each showed excellent stability and reusability for their respective catalytic process. Lately, Ni@porous silica-shell[32], Ni@SiO_2 yolkshell nanoreactor[33], and Ni-Yolk@Ni@SiO_2 nanocomposites[34] have been established in reforming of methane and outlined core-shell or yolk-shell structures were effective against active particle agglomeration at high temperature. However, their Ni wt.% loading was comparatively high for the reaction and among them Ni-Yolk@Ni@SiO_2 nanocomposites have the suitable Ni loading. Also, the permeation degree of the respective shells was varied and influenced their yield of conversion of methane to syngas. SiO_2 as shell support was shown to be effective in their respective reaction, however, the stability under water or water vapour is rather poor at high temperature.[35, 36] Motivated by these studies, we developed a catalyst with high stability for steam reforming of methane reaction with relatively low Ni loading while effectively isolating active Ni particles.

In this paper, we report a Ni@yolk-ZrO_2 catalyst synthesized via double template emulsion method by varying the porosity of ZrO_2 hollow shell to investigate the catalytic performance and their stability in steam reforming of methane.

2. Experimental

2.1 Synthesis and characterization

Synthesis of Ni colloids and Ni@SiO_2. The synthesis of Ni@SiO_2 colloids was carried out by reverse micelle approach. Typically, 3mL of aqueous 0.25M $NiCl_2$ and 11.5mL of Brij L4 (Sigma-Aldrich) were mixed with 40mL of n-octane in a 250mL 3-neck round bottom flask at 30^{o}C under N_2 atmosphere protection. The mixture was stirred for 10 min before 1mL of 3.172M ice-cooled $NaBH_4$ solution was quickly dropped into the flask. Immediately, a clear solution would turn pitch black and bubbles were generated. After 5 minutes of N_2 purge, the flask was sealed. Subsequently the solution was stirred for 12 hours to form stable Ni colloids. The SiO_2 coating was achieved by subsequently adding 50mL of n-octane, 2.4mL Brij L4, 1.2mL ammonia (26%-28%), 2mL of TEOS into the solution and kept stirring for 3 hours. After 3 hours, additional 2mL of TEOS was added and stirred for another 5 hours. The Ni@SiO_2 colloids was obtained after centrifuge and washed with acetone and ethanol, then re-dispersed into 40mL of ethanol.

Synthesis of Ni@SiO_2@ZrO_2. 35mL of dispersed Ni@SiO_2 colloids in ethanol was used for the subsequent synthesis by mixing with 0.6mL Brij L4, 0.6mL H_2O in 220mL of ethanol and stirred for 30 minutes. Then, 2mL of $Zr(OBu)_4$ was added and vigorously stirred for 8hours at 30^{o}C. The colloids were washed with ethanol twice and re-dispersed into 40mL deionized water with 0.001M $NaBH_4$ and aged for 3 days. The powder was collected and dried under 105^{o}C for 3 hours and calcined at 750^{o}C (2^{o}C/min) for 3 hours.

Synthesis of Ni@yolk-ZrO_2. The calcined powder was dispersed into 40mL of 3M NaOH solution and stirred for 48 hours under stirring. The colloids were washed with deionized water several times. After drying at 105^oC for 3 hours, the powder was calcined at 550^oC. Subsequently, the obtained powder was reduced under 10%H_2/Ar at 650^oC for 3 hours. During synthesis of Ni@SiO_2@ZrO_2, varying addition of Brij L4 from 0.0mL, 0.4mL, 0.6mL, 0.8, 1.2mL will be denoted as BrNi-0.0, BrNi-1.6, BrNi-2.4, BrNi-3.2, and BrNi-4.8 respectively as the mole ratio of Brij L4-to-Ni.

Synthesis of Ni/ZrO_2. 1g of commercially made ZrO_2 powder (TOSOH) was impregnated with 50mL of 0.017M NiCl and stirred under room temperature. After 6 hours, the obtained sol was dried at 100 ^oC for 3 hours and subsequently calcined at 750 ^oC for 3 hours, followed by reduction under 10%H_2/Ar at 650^oC for 3 hours.

X-ray diffraction patterns were recorded using Bruker D8 Advance with Cu-Kα radiation (λ = 1.5418 Å) in the 2θ range of 10^o-90^o. Transmission electron microscopy (TEM), model JEM 2100 was used to study the morphology and microstructure of the catalyst. The TEM specimens were prepared by dropping a trace amount of the sample dispersed in ethanol on a carbon coated copper grid (300 mesh). The BET surface area measurement was carried out using a Micrometrics ASAP 2020M apparatus at 77 K. Prior to the measurement, the sample was degassed at 300^oC for 5 h under vacuum. Temperature-programmed reduction (FINESORB3010E, Zhejiang Fintec Co.) was performed to determine the nickel species and its reducibility for each catalyst. Typically, catalyst was filled into a U-shape quartz tube and held by quartz wool. Prior to reduction, the sample was treated with pure Ar for 30 min at 300^oC to remove any impurities. The sample tube was then cooled down to room temperature. 10%H_2/Ar (25mLmin^{-1}) was introduced, and the temperature was increased from room temperature to 800^oC with a heating rate of 5$^oC min^{-1}$. X-ray photoelectron spectroscopy (XPS) spectra were recorded on a Shimadzu Axis Ultradld

spectroscope (Japan) using the monochromatized Al Kα radiation resource at room temperature and under a vacuum of 10^{-7} Pa (10^{-9} Torr). The starting angel of the photoelectron was set at 90°. The spectrum was calibrated with a C 1s spectrum of 248.8 eV.

2.2 Catalytic evaluation

Steam reforming of methane was studied in a fixed bed quartz reactor (12mm ID) under atmospheric pressure. The reactor was equipped with a pre-heater, a syringe pump, a cold condenser and a gas flow meter. 100mg of catalyst diluted with filled quartz sand of 2cm length was used. The quartz reactor loaded with catalyst was heated in an electric furnace and the temperature of the bed was controlled by a K-type thermocouple positioned at the center of the catalyst bed. Prior to the test, the catalyst was reduced *in situ* 650°C with 10%H_2/Ar mixture (50 $mLmin^{-1}$) for 3 h. A reaction mixture of H_2O and CH_4 (Steam to carbon molar ratio of 2.5:1) without dilution was fed using a gas hourly space velocity (GHSV) of 50,400 $mLg_{cat}^{-1}h^{-1}$. The effluent gases were analyzed by an on-line gas chromatography (INESA Scientific Instrument Co.Ltd, GC-122) equipped with a packed column (TDX-01) and a TCD detector. A cold trap was placed before the TCD to remove moisture in the gas products. The peak area normalization method was used for quantitative analysis of effluent gaseous.[37, 38] The CH_4 conversion and CO selectivity were calculated using equations (1) and (2) as follows:

$$X_{CH_4}(\%) = \frac{[CO] + [CO_2]}{[CO] + [CO_2] + [CH_4]} \times 100 \qquad (1)$$

$$CO\ selectivity\ (\%) = \frac{[CO]}{[CO] + [CO_2]} \times 100 \qquad (2)$$

3. Results and discussion

XRD patterns of the catalyst are shown in Fig. 1a. The Ni@yolk-ZrO_2 catalyst shows a low crystallinity of Ni metal compared to impregnated Ni/ZrO_2 catalyst. The catalysts showed the characteristic peaks of tetragonal ZrO_2 and Ni metal. The peaks observed at $2\theta = 44.5^o$, 51.8^o, and 76.4^o can be assigned to the (111), (200), (220) planes of Ni metal, respectively. The average crystallite size of Ni was determined by the peak broadening of the (111) reflection in the XRD patterns, using the Scherrer formula, and their respective crystallite size will are shown in Table 1. The Scherrer equation was used to calculate the crystallite size and compared with the particle size results obtained from the TEM study. This would help to give insight if increasing the surfactant concentration would affect the crystallite size. However, BrNi-4.8 has a relatively sharp peak of Ni at $2\theta = 44.5^o$. ZrO_2 at $2\theta = 30.5^o$ has largest crystallite size among the catalysts excluding the reference sample Ni/ZrO_2. This indicates that excess addition of surfactant Brij L4, disfavours the dispersion of the Ni active metals in the ZrO_2 nano-framework. Also, the ZrO_2 grains in BrNi-4.8 were larger than other configurations.

The TEM micrographs of Ni@yolk-ZrO_2 catalysts before steam reforming test are shown in Fig. 2. The Ni particles are uniformly distributed in the ZrO_2 hollow shell and no apparent aggregation of particles was observed. The particle distribution of Ni in each catalyst is shown in Table 1. It was observed that increased addition of surfactant increased the Ni nanoparticle size. The surfactant was employed as porosity agent to achieve permeation of gaseous exchange for the ZrO_2 hollow shell. The increase in Ni particle size with surfactant addition could be related to the total pore volume in the catalysts. Among the pore volumes, BrNi-4.8 has the lowest value of 0.18 cm^3g^{-1}. Liu reported that for suppressing agglomeration of active metal nanoparticles, the substrates must possess two key properties; the uniformity of the active metal particles, and abundance of micropores on

the support.[39] The aspects of high uniformity of active metal nanoparticles were achieved, as observed by TEM. Subsequently, the catalysts (except BrNi-4.8) have moderately high total pore volumes of above 0.40 cm^3g^{-1}, which indicates that the synthesized catalysts were able to suppress the agglomeration of the active metal nanoparticles. Also, the structural integrity of BrNi-4.8 collapsed after steam reforming test (Fig. 3e), which implies that excessive addition of surfactant in Ni@yolk-ZrO_2 catalyst resulted in a fragile ZrO_2 hollow shell.

The BET isotherm graph (Fig. 1b) showed Ni@yolk-ZrO_2 catalyst have Type-IV isotherm characteristic and hysteresis loop of category H3 except in the case of BrNi-4.8, with hysteresis loop of category H2. It shows that the addition of surfactant leads to pores generation in the ZrO_2 hollow shell matrix. The TEM micrographs of all Ni@yolk-ZrO_2 catalyst have similar yolk-shell structures; however, the pore distributions were not similar. From Fig 4, all the highest pore distributions of the catalysts were situated around 18nm except BrNi-4.8, which presented the highest pore distribution situated at 4 nm. It was noted from TEM micrograph (Fig. S1) that the void space of Ni core and the ZrO_2 hollow shell was 19nm. This indicated that excessive addition of surfactant enlarged the pores existing in the ZrO_2 hollow shell and resulted in channelled mesoporous characteristic in BET isotherm graph. Besides, the increasing addition of the surfactant Brij L4 lead to gradual interconnecting the pores of ZrO_2 hollow shell, which affects the pores structure developed from slit-shape to ink bottle, thus influences the catalysts' efficiency. On the other hand, weak integrity of the ZrO_2 hollow shell could be ascribed to the hydrothermal instability of SiO_2 contributed in the shell matrix. From Table 2, BrNi-4.8 before and after steam reforming test showed drastic changes in Si 2p mass concentration over the catalyst surface when compared to other configurations. In addition, the O 1s XPS spectra from Fig. 5 of ZrO_2 (530 eV) and SiO_2 (532 eV) showed that before testing, SiO_2 was detected as lower intensity than ZrO_2, and higher intensity after test. This implied that SiO_2 entities/matrix were disrupted in the shell and detected on the surface

of the catalyst. It was proposed that SiO_2 was not a good selection as support in steam reforming methane due to hydrothermal instability at high temperature.

Fig. 6 shows the Ni 2p XPS peak of Ni@yolk-ZrO_2 catalysts before and after steam reforming test. Before steam reforming test, Ni particles were detectable over the catalyst surface. In contrast, after testing, these showed almost non-existence of Ni particles over the catalyst surface, with the exception of the configuration of BrNi-4.8 catalyst. From XPS depth analysis, Ni particles have been detected partly in the matrix of ZrO_2 hollow shell before testing and inside the hollow shell after steam reforming of methane testing. As for BrNi-4.8 catalyst, it still displayed trace of Ni 2p mass concentration, while after steam reforming tests it was observed that Ni particles were not successfully encapsulated in the ZrO_2 hollow shell. Validation from TEM micrograph from Fig. 3e showed the structural framework of BrNi-4.8 catalyst was collapsed after steam reforming test. It is possible to conclude that excessive addition of surfactant resulted in weak integrity of ZrO_2 hollow shell which affected the stability of the catalyst during steam reforming of methane.

TPR analysis was carried out to evaluate the active Ni metal interaction with the ZrO_2 hollow shell support. As increasing addition of surfactant resulted in weaker ZrO_2 support, it lead to ease of mobility for Ni particles in the catalyst. Fig. 7 showed the patterns of reducibility of Ni in their configurations as of Ni@yolk-ZrO_2. BrNi-0.0 has highest 1^{st} peak reduction temperature and gradually decreases to lower reduction temperature as addition of surfactant increased. The reducibility of the 2^{nd} reduction peak gradually decrease to lower reduction temperature, as strong metal-support interactions between Ni species and Zr species weaken due to the total pore volume decreased and the anchoring effect no longer sturdy to support the Ni particle. This indicated the amount of surfactant addition modifies the existing Ni species in the catalyst. From BET isotherm graph, the onset of capillary condensation was shifting to lower relative pressure, showing that the pores in the

ZrO_2 hollow shell were enlarged as addition of surfactant increased. It was evident from TPR testing that Ni species were affected by the pores of ZrO_2 hollow shell.

3.1 Catalytic evaluation

The catalytic steam reforming of methane of Ni@yolk-ZrO_2 catalysts and impregnated catalysts as reference sample were studied at GHSV of 50,400 $mLg_{cat}^{-1}h^{-1}$ and S/C=2.5 at 750^{o}C, and the results are shown in Fig. 8. The methane conversion of Ni@yolk-ZrO_2 catalysts increased with time and the conversions were stable at 90% with time on stream, except BrNi-0.0 and BrNi-4.8. Initially, BrNi-0.0 showed high conversion of methane at 90% and dropped to 80% after 24 hours. The drop in conversion could be related to the low amount of micropores in the ZrO_2 hollow shell which does not support the gaseous exchange during steam reforming test. As for BrNi-4.8, the low conversion was ascribed to the relative large Ni particles size when compared with other configurations and its weak integrity framework of ZrO_2 hollow shell.

Analysing the performances of the superior performance of these catalysts, the Ni particles size played an important role in the performance in steam reforming of methane. Comparing BrNi-2.4 with BrNi-4.8, with Ni particles size of 9 nm and 11.1nm respectively, which greatly affected the methane dissociation during steam reforming test. Another factor was the yolk-shell structure, which was stable after 48 hours of testing for BrNi-2.4, whereas the yolk-shell structure of BrNi-4.8 collapsed after 24 hours. The XPS Ni 2p and TEM images after catalytic test showed the zirconia hollow shell effectively isolating the Ni particles with high structural stability, and maintaining high performance in steam reforming of methane. The overall performance was low for BrNi-4.8 due to the weak integrity framework of ZrO_2 hollow shell. XPS and TEM showed the entities of SiO_2 were greatly increased on the surface of the catalyst which indicating the destruction of the ZrO_2 hollow shell. As for BrNi-0.0, the performance was slightly lower than BrNi-1.6, BrNi-2.4, and BrNi-3.2. The inhibition of the

performance of BrNi-0.0 was ascribed to the physical characteristics of its ZrO_2 hollow shell. It showed a high amount of total pore volume but has low amount of micropore volume, indicating the low amount of slit-shaped pores in the ZrO_2 hollow shell, which was limiting the gaseous exchange in steam reforming test. Also, the slit-shaped pores could be diminished due to sintering of ZrO_2 nano-grains in the ZrO_2 hollow shell, limiting the diffusion of reactants or products during steam reforming of methane.

4. Conclusions

Ni@yolk-ZrO_2 nanoparticles with sub-10nm Ni cores were synthesized via a double template method and evaluated for steam reforming of methane. Active Ni particles agglomeration behaviour was studied by varying the pore size of ZrO_2 hollow shell with surfactant addition. It was shown that the surfactant additions directly affected the physical properties of ZrO_2 hollow shell and consequently their catalytic performance. Without surfactant addition, the ZrO_2 hollow shell limited the permeation of gases during reaction, whereas, adequate addition of surfactant promotes gaseous exchange. Over addition of surfactant resulted in weak ZrO_2 hollow shell. Besides, from XPS analysis, the hydrothermal stability of the catalysts was observed to be moderately strong in steam reforming of methane which favours long hours of reaction. It is notable that the catalysts have both anti-agglomerating and good hydrothermal stability which is possible to extend to other similar reactions.

Acknowledgements

This work is supported by the National Basic Research Program of China (2013CB934800), Zhejiang Province Natural Science Foundation (LY15B030005), and the Innovation Team Foundation (2014B81004) from the Ningbo Science and Technology Bureau. ZYL acknowledged the scholarship awarded by the University of Nottingham, Ningbo China.

Notes and references

1. G. A. Olah, A. Goeppert, M. Czaun and G. K. S. Prakash, *Journal of the American Chemical Society*, 2013, 135, 648-650.

2. A. P. Simpson and A. E. Lutz, *International Journal of Hydrogen Energy*, 2007, 32, 4811-4820.

3. G. Jones, J. G. Jakobsen, S. S. Shim, J. Kleis, M. P. Andersson, J. Rossmeisl, F. Abild-Pedersen, T. Bligaard, S. Helveg, B. Hinnemann, J. R. Rostrup-Nielsen, I. Chorkendorff, J. Sehested and J. K. Nørskov, *Journal of Catalysis*, 2008, 259, 147-160.

4. Z. Hou and T. Yashima, *Applied Catalysis A: General*, 2004, 261, 205-209.

5. N. Sun, X. Wen, F. Wang, W. Wei and Y. Sun, *Energy & Environmental Science*, 2010, 3, 366-369.

6. L. Pino, A. Vita, F. Cipitì, M. Laganà and V. Recupero, *Applied Catalysis B: Environmental*, 2011, 104, 64-73.

7. V. R. Choudhary, K. C. Mondal and A. S. Mamman, *Journal of Catalysis*, 2005, 233, 36-40.

8. R. B. Duarte, O. V. Safonova, F. Krumeich, M. Makosch and J. A. van Bokhoven, *ACS Catalysis*, 2013, 3, 1956-1964.

9. N. Laosiripojana and S. Assabumrungrat, *Applied Catalysis B: Environmental*, 2005, 60, 107-116.

10. G. Jacobs, R. A. Keogh and B. H. Davis, *Journal of Catalysis*, 2007, 245, 326-337.

11. D.-W. Jeong, H.-S. Na, J.-O. Shim, W.-J. Jang, H.-S. Roh, U. H. Jung and W. L. Yoon, *International Journal of Hydrogen Energy*, 2014, 39, 9135-9142.

12. H. Yin, Z. Ma, H. Zhu, M. Chi and S. Dai, *Applied Catalysis A: General*, 2010, 386, 147-156.

13. Z.-j. Wang, Y. Xie and C.-j. Liu, *The Journal of Physical Chemistry C*, 2008, 112, 19818-19824.

14. S. Sokolov, E. V. Kondratenko, M.-M. Pohl, A. Barkschat and U. Rodemerck, *Applied Catalysis B: Environmental*, 2012, 113–114, 19-30.

15. J. Sehested, J. A. P. Gelten, I. N. Remediakis, H. Bengaard and J. K. Nørskov, *Journal of Catalysis*, 2004, 223, 432-443.

16. J. Sehested, *Catalysis Today*, 2006, 111, 103-110.

17. D. Liu, R. Lau, A. Borgna and Y. Yang, *Applied Catalysis A: General*, 2009, 358, 110-118.

18. J. C. Guevara, J. A. Wang, L. F. Chen, M. A. Valenzuela, P. Salas, A. García-Ruiz, J. A. Toledo, M. A. Cortes-Jácome, C. Angeles-Chavez and O. Novaro, *International Journal of Hydrogen Energy*, 2010, 35, 3509-3521.

19. S. Zhang, S. Muratsugu, N. Ishiguro and M. Tada, *ACS Catalysis*, 2013, 3, 1855-1864.

20. M. Lindo, A. J. Vizcaíno, J. A. Calles and A. Carrero, *International Journal of Hydrogen Energy*, 2010, 35, 5895-5901.

21. J. Park and H. Song, *Nano Res.*, 2011, 4, 33-49.

22. Y. Liu, Z. Fang, L. Kuai and B. Geng, *Nanoscale*, 2014, 6, 9791-9797.

23. G. Li and Z. Tang, *Nanoscale*, 2014, 6, 3995-4011.

24. V. Evangelista, B. Acosta, S. Miridonov, E. Smolentseva, S. Fuentes and A. Simakov, *Applied Catalysis B: Environmental*, 2015, 166–167, 518-528.

25. Q. Zhang, W. Wang, J. Goebl and Y. Yin, *Nano Today*, 2009, 4, 494-507.

26. Q. Sun, X.-Q. Zhang, Y. Wang and A.-H. Lu, *Chinese Journal of Catalysis*, 2015, 36, 683-691.

27. J. Liu, S. Z. Qiao, J. S. Chen, X. W. Lou, X. Xing and G. Q. Lu, *Chemical Communications*, 2011, 47, 12578-12591.

28. H.-L. Jiang, T. Umegaki, T. Akita, X.-B. Zhang, M. Haruta and Q. Xu, *Chemistry – A European Journal*, 2010, 16, 3132-3137.

29. S. H. Joo, J. Y. Park, C.-K. Tsung, Y. Yamada, P. Yang and G. A. Somorjai, *Nat Mater*, 2009, 8, 126-131.

30. X. Huang, C. Guo, J. Zuo, N. Zheng and G. D. Stucky, *Small*, 2009, 5, 361-365.

31. J. B. Joo, M. Dahl, N. Li, F. Zaera and Y. Yin, *Energy & Environmental Science*, 2013, 6, 2082-2092.

32. L. Li, S. He, Y. Song, J. Zhao, W. Ji and C.-T. Au, *Journal of Catalysis*, 2012, 288, 54-64.

33. J. C. Park, J. U. Bang, J. Lee, C. H. Ko and H. Song, *Journal of Materials Chemistry*, 2010, 20, 1239-1246.

34. Z. Li, L. Mo, Y. Kathiraser and S. Kawi, *ACS Catalysis*, 2014, 4, 1526-1536.

35. H. Xiong, H. N. Pham and A. K. Datye, *Green Chemistry*, 2014, 16, 4627-4643.

36. M. Kanezashi and M. Asaeda, *Journal of Membrane Science*, 2006, 271, 86-93.

37. Q. Wang, X. Li, W. Li and J. Feng, *Catalysis Communications*, 2014, 50, 21-24.

38. X. Li, J. Feng, H. Fan, Q. Wang and W. Li, *Catalysis Communications*, 2015, 59, 104-107.

39. Z. Liu, R. Che, A. A. Elzatahry and D. Zhao, *ACS Nano*, 2014, 8, 10455-10460.

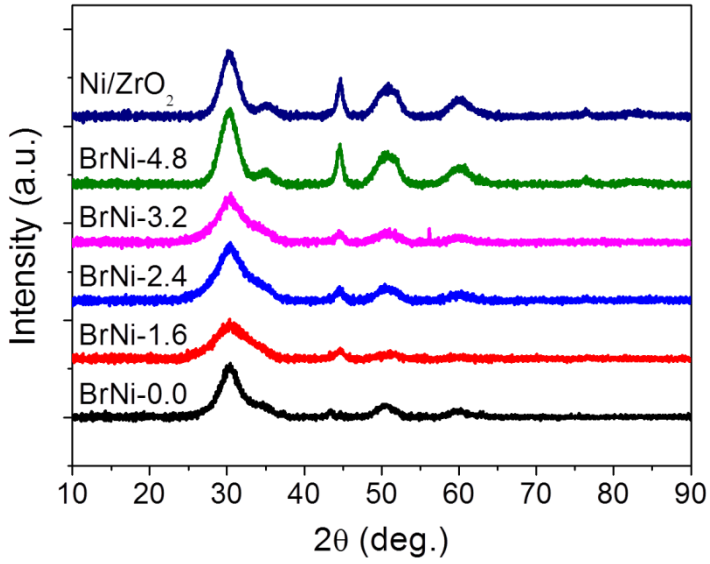

(a)

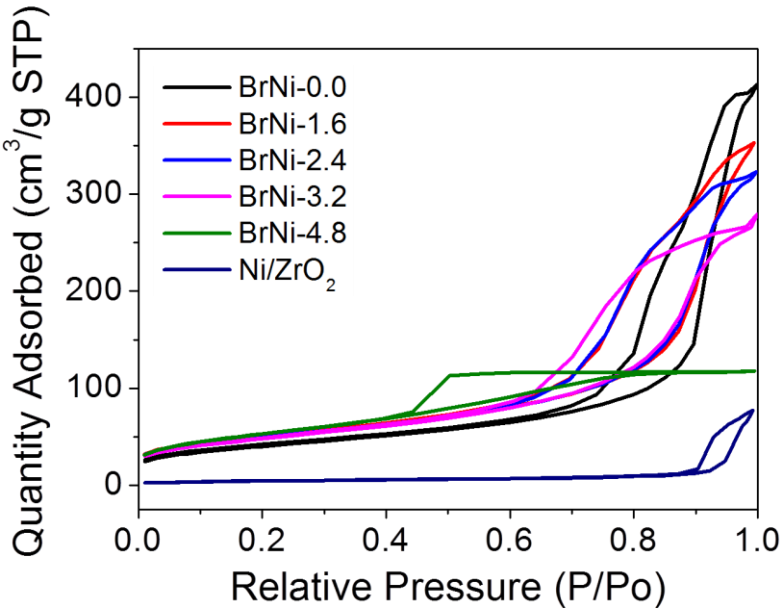

(b)

Fig 1. XRD patterns (a) and BET isotherm (b) of Ni@yolk-$ZrO_2$and Ni/ZrO_2 catalysts.

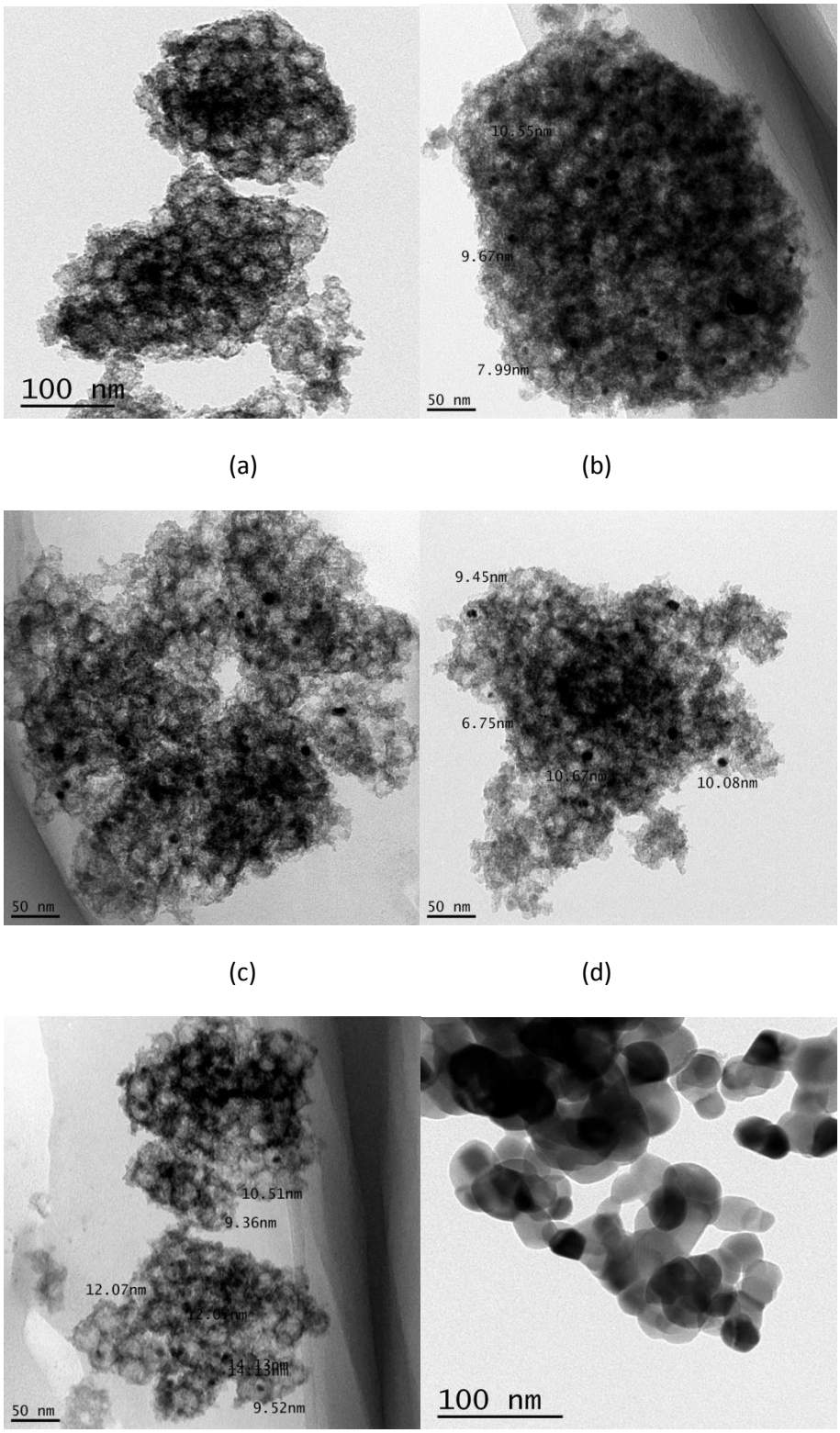

Fig 2. TEM images of BrNi-0.0 (a), BrNi-1.6 (b), BrNi-2.4 (c), BrNi-3.2 (d), BrNi-4.8 (e), and Ni/ZrO_2 (f) before steam reforming test.

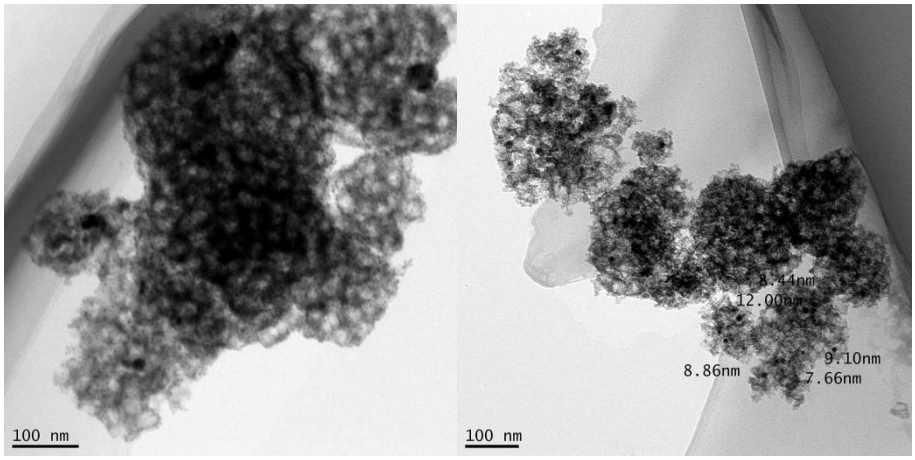

(a) (b)

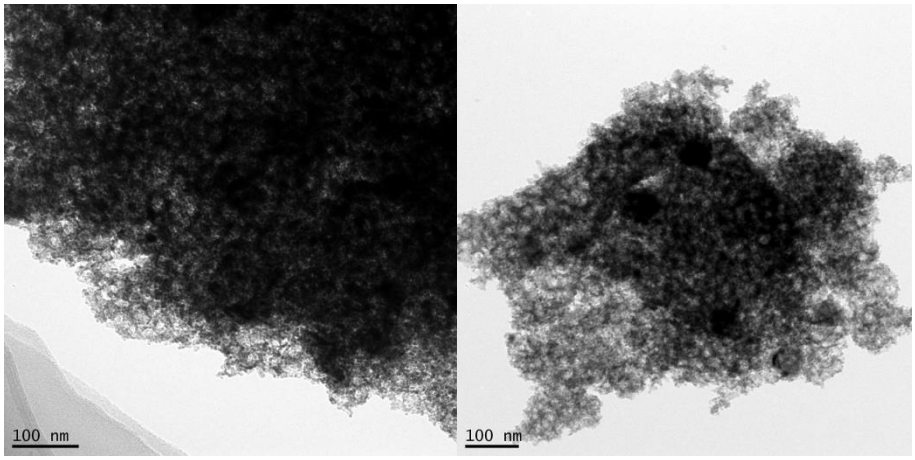

(c) (d)

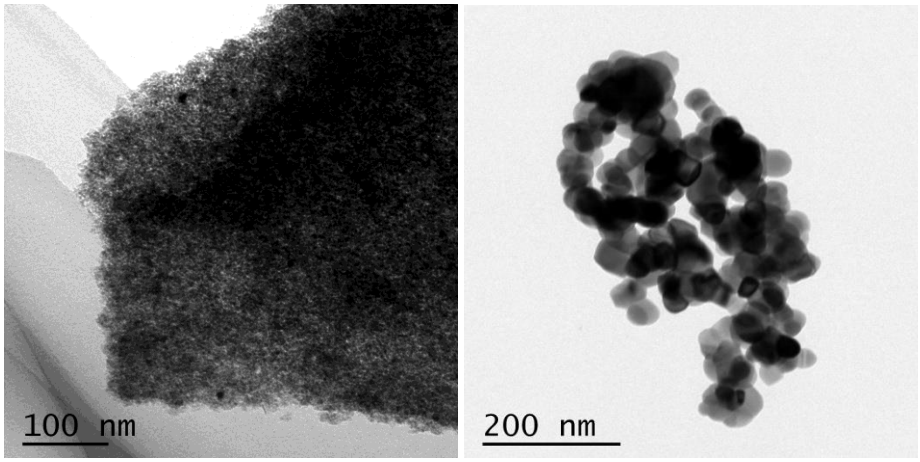

(e) (f)

Fig 3. TEM images of BrNi-0.0 (a), BrNi-1.6 (b), BrNi-2.4 (c), BrNi-3.2 (d), BrNi-4.8 (e), and Ni/ZrO_2 (f) after steam reforming test.

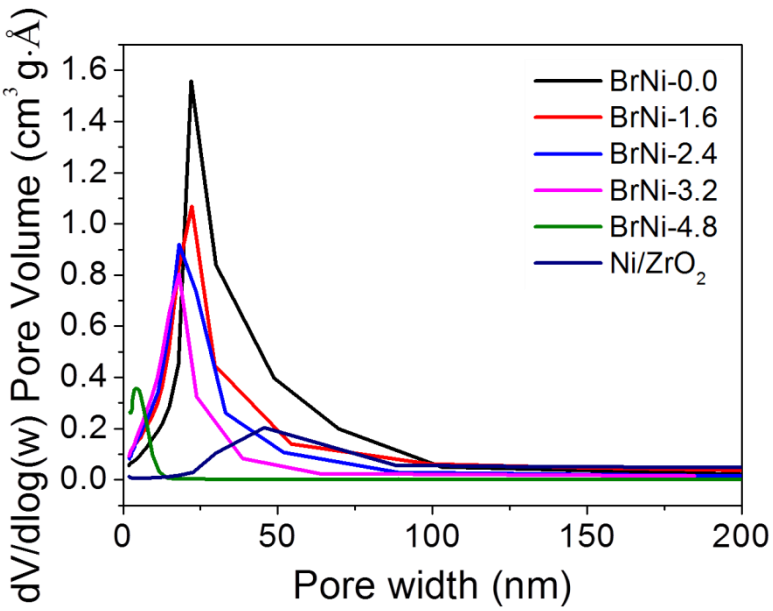

Fig 4. Pore size distribution of Ni@yolk-ZrO_2 catalysts and impregnated Ni/ZrO_2 catalyst.

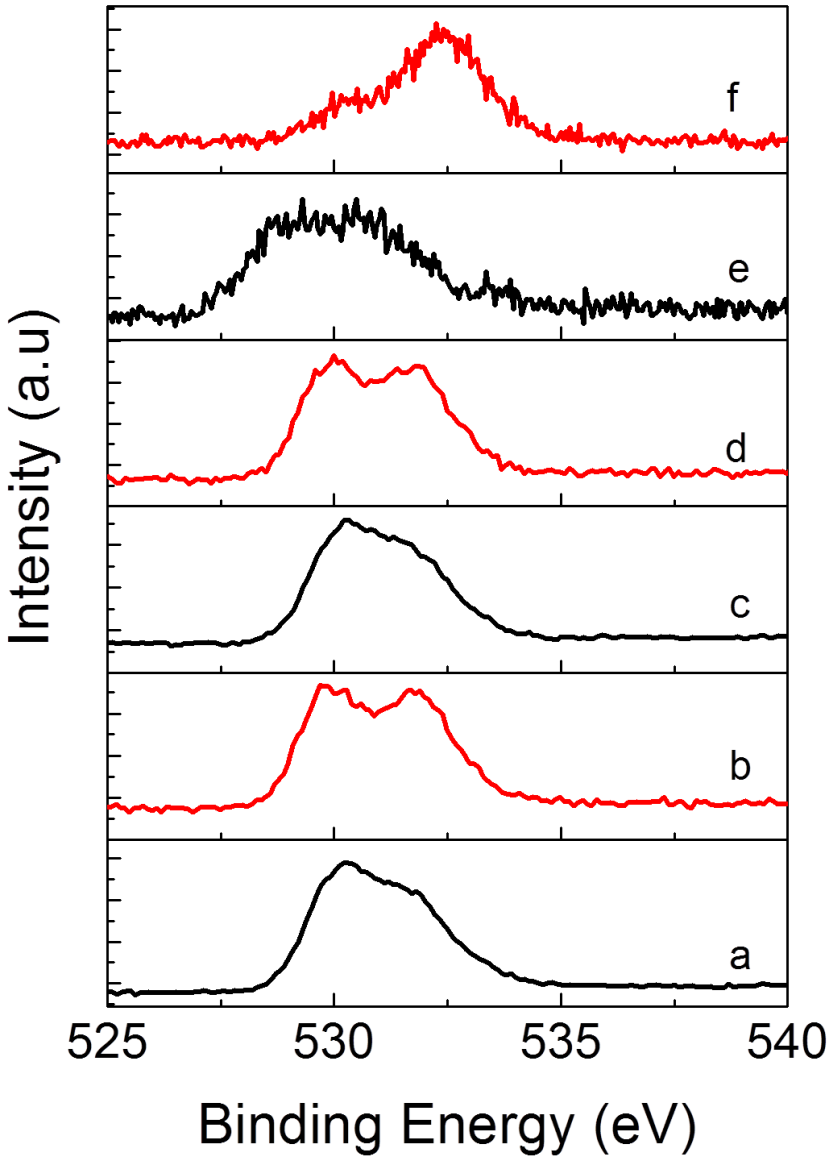

Fig 5. XPS O 1s spectra before (black line) and after (red line) steam reforming test of BrNi-0.0 (a, b), BrNi-2.4 (c, d), and BrNi-4.8 (e, f) samples

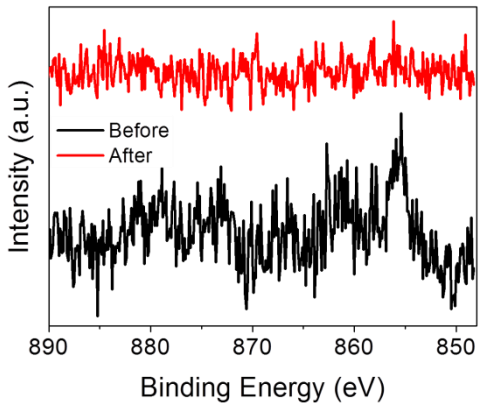

(a)

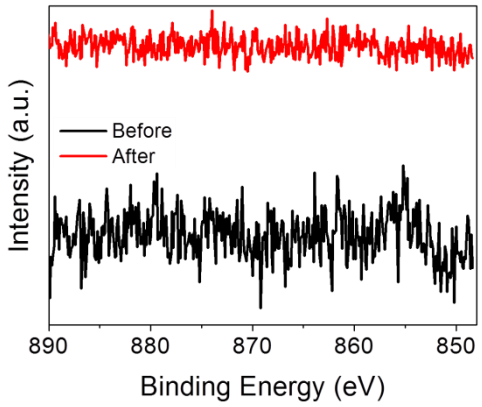

(b)

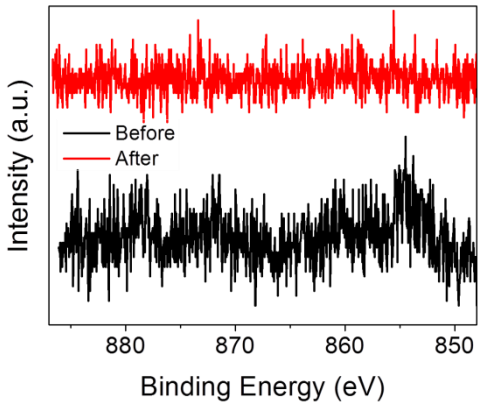

(c)

Fig 6. XPS selected scan of Ni 2p signal of BrNi-0.0 (a), BrNi-2.4 (b), and BrNi-4.8 (c) before and after steam reforming test.

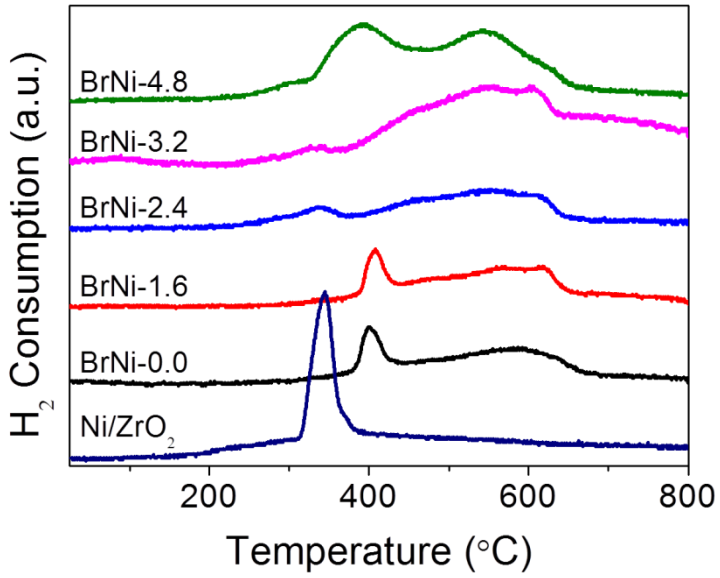

Fig 7. Temperature-programmed reduction profile of Ni@yolk-ZrO_2 catalysts.

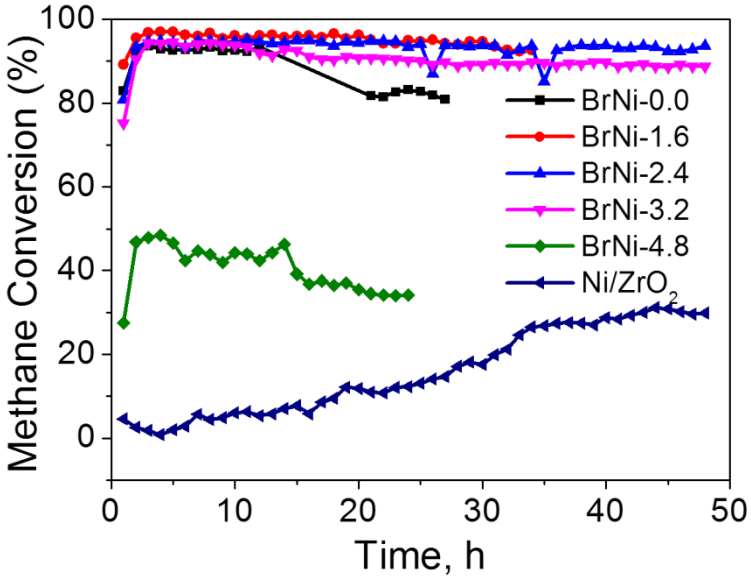

(a)

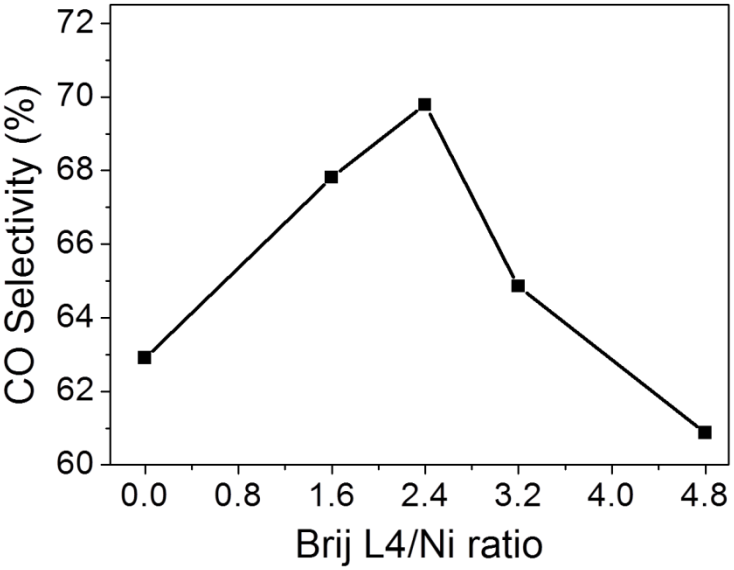

(b)

Fig 8. Catalytic performance of steam reforming of methane on Ni@yolk-ZrO_2 and Ni/ZrO_2 catalysts (a). CO selectivity of Ni@yolk-ZrO_2 catalysts (b) at last point of reaction time.